 CMES, vol.65, no.3, pp.217-244, 2010

A Dual-Reciprocity Boundary Element Simulation of Axisymmetric Dual-Phase-Lag Heat Conduction in Nonhomogeneous Media

B.I. Yun[1] **and W.T. Ang**[1,2]

Abstract: A dual-reciprocity boundary element method is proposed for simulating numerically axisymmetric dual-phase-lag heat conduction in nonhomogeneous thermally isotropic media. The properties of the media, such as thermal conductivity and specific heat, are assumed to vary continuously in space. To check its validity and assess its accuracy, the proposed method is first applied to solve some specific test problems with known solutions. It is then used to simulate the axisymmetric dual-phase-lag heat conduction in a particular nonhomogeneous medium subject to a concentrated surface heating. The effects of the dual phase lags and the spatial variations of the thermal properties of the medium on the temperature distribution are examined.

Keywords: Boundary element method, dual-reciprocity method, axisymmetric heat conduction, dual-phase-lag heat model, nonhomogeneous media.

1 Introduction

The classical Fourier heat flux model which assumes that the heat flux is instantaneously proportional to the temperature gradient of the thermal field leads to the physically undesirable prediction that thermal waves travel at an infinite speed. A frequently used justification for using the model is that the wave nature of heat conduction is important only over a very short period of time or under extreme conditions such as at very low temperature or at a very high rate of heat flow. Nevertheless, thermal waves might possibly be observed in solids even at normal room temperatures as reported in Kaminski (1990), and Yuen and Lee (1989) showed that it is possible that they may last over a relatively long period of time. The Fourier model cannot be used effectively to capture the effects of microscopic phenomena,

[1] Division of Engineering Mechanics, School of Mechanical and Aerospace Engineering, Nanyang Technological University, Singapore.
[2] Author for correspondence (mwtang@ntu.edu.sg).

such as phonon scattering and phonon-electron interaction, on heat transfer. Such effects may be of importance in many micro-engineering applications involving dielectric films, insulators and semiconductors.

The dual-phase lag model proposed by Tzou (1995, 1997) has been successfully employed in the analyses of certain thermal problems (see, for example, Antaki, 1998; Tang and Araki, 1991; and Tzou and Chiu, 2001). To account for thermal waves and microscopic effects, the model modifies the classical Fourier constitutive equation by introducing very small time delays in the temperature gradient and the heat flux. The heat equation together with the dual-phase-lag constitutive equation gives rise to a relatively more complicated governing partial differential equation which contains third order partial derivatives of the unknown temperature. The numerical solution of the partial differential equation subject to appropriate initial-boundary conditions is a subject of considerable interest among many researchers. For example, Manzari and Manzari (1998) had solved a special case of the equation (that is, for the case of zero time delay in the temperature gradient) using the finite-element method, Dai and Nassar (1999), Zhang and Zhao (2001) and Pan, Tang and Zhou (2006) had outlined finite difference schemes for the equation in one- and two-dimensional solution domains, and Ang (2002) had proposed a boundary element method for two-dimensional dual-phase-lag heat conduction in homogeneous solids.

The present paper presents a dual-reciprocity boundary element approach for simulating numerically axisymmetric dual-phase-lag heat conduction in nonhomogeneous thermally isotropic media with properties which vary continuously in space. In the numerical approach here, the governing partial differential equation is first converted into a suitable integro-differential equation. In addition to a boundary integral over a curve on the axisymmetric coordinate plane, the integro-differential equation also contains a domain integral. The dual-reciprocity approach pioneered by Brebbia and Nardini (1983) is used together with the interpolating functions in Yun and Ang (2010) to express the domain integral approximately in terms of a boundary integral. The boundary of the solution domain is discretized into many small elements, the temperature and heat flux are approximated as functions which vary linearly across a boundary element and the time derivatives of the temperature and the heat flux in the integro-differential formulation are suppressed by using the Laplace transform. The problem is eventually reduced to solving a system of linear algebraic equations. Once the linear algebraic equations are solved, the temperature in the physical space can be approximately recovered by a numerical method for inverting Laplace transforms.

To check its validity and assess its accuracy, the numerical procedure presented here is first applied to solve some specific test problems with known solutions.

It is then used to simulate the axisymmetric dual-phase-lag heat conduction in a particular nonhomogeneous medium subject to concentrated surface heating. The effects of the dual phase lags and the spatial variations of the thermal properties of the medium on the temperature distribution are examined.

The problem under consideration here is of practical interest as heat transfer in many engineering and biological systems can be modeled as axisymmetric and functionally graded solids with material properties which may be regarded as continuously varying in space are nowadays widely used in engineering applications. The analysis of functionally graded materials has always been a subject of considerable interest among many researchers (see, for example, Divo and Kassab, 1998; Park and Ang, 2000; Azis, Clements and Budhi, 2003; Nerantzaki and Kandilas, 2008;; Sladek, Sladek and Solek, 2009; Ochiai, Sladek and Sladek, 2009; Ding, Li and Zhou, 2010). In recent years, the dual-phase-lag model is used in the analysis of heat transfer in biological tissues (Zhou, Zhang and Chen, 2009; and Zhou, Chen and Zhang, 2009).

2 Dual-phase-lag heat conduction

According to the dual-phase-lag heat model proposed by Tzou (1995, 1997), the heat flux $\underline{\mathbf{q}}$ in a heat conducting medium is related to the temperature distribution T by

$$\underline{\mathbf{q}}(\underline{\mathbf{x}},t+\tau_q) = -\kappa \underline{\nabla} T(\underline{\mathbf{x}},t+\tau_T), \tag{1}$$

where x denotes the position of a point in the medium, t is time, κ is the thermal conductivity, $\underline{\nabla}$ is the nabla (gradient) operator and τ_q and τ_T are small magnitude time parameters giving the phase lags of the heat flux components and the temperature gradient respectively. A somewhat detailed discussion of the dual-phase-lag model can also be found in the book by Zhang (2007).

If the left and right hand sides of (1) are expanded as Taylor-Maclaurin series about $\tau_q = 0$ and $\tau_T = 0$ respectively, then ignoring second and higher order terms in τ_q and τ_T (that is, assuming that the phase lags are sufficiently small) gives

$$\underline{\mathbf{q}}(\underline{\mathbf{x}},t) + \tau_q \frac{\partial}{\partial t}[\underline{\mathbf{q}}(\underline{\mathbf{x}},t)] = -\kappa \underline{\nabla}(T(\underline{\mathbf{x}},t) + \tau_T \frac{\partial}{\partial t}[T(\underline{\mathbf{x}},t)]). \tag{2}$$

The use of (2) together with the energy equation

$$-\underline{\nabla} \bullet (\underline{\mathbf{q}}(\underline{\mathbf{x}},t)) + Q = \rho c \frac{\partial}{\partial t}[T(\underline{\mathbf{x}},t)]) \tag{3}$$

yields

$$\underline{\nabla} \bullet (\kappa \underline{\nabla}(T(\underline{\mathbf{x}},t) + \tau_T \frac{\partial}{\partial t}[T(\underline{\mathbf{x}},t)])) = \rho c(\frac{\partial}{\partial t}[T(\underline{\mathbf{x}},t)] + \tau_q \frac{\partial^2}{\partial t^2}[T(\underline{\mathbf{x}},t)]) - (Q + \tau_q \frac{\partial Q}{\partial t}), \quad (4)$$

where ∇^2 is the Laplacian operator and ρ and c are the volume density and the specific heat of the solid and Q is the internal heat generation rate.

If the internal heat generation rate is of the form

$$Q = A(\underline{\mathbf{x}})T(\underline{\mathbf{x}},t) + B(\underline{\mathbf{x}},t), \quad (5)$$

where $A(\underline{\mathbf{x}})$ and $B(\underline{\mathbf{x}},t)$ are given functions, (4) can be written as

$$\underline{\nabla} \bullet (\kappa \underline{\nabla}(T(\underline{\mathbf{x}},t) + \tau_T \frac{\partial}{\partial t}[T(\underline{\mathbf{x}},t)])) = \rho c \tau_q \frac{\partial^2}{\partial t^2}[T(\underline{\mathbf{x}},t)] + (\rho c - \tau_q A(\underline{\mathbf{x}})) \frac{\partial}{\partial t}[T(\underline{\mathbf{x}},t)] - (A(\underline{\mathbf{x}})T(\underline{\mathbf{x}},t) + B(\underline{\mathbf{x}},t) + \tau_q \frac{\partial}{\partial t}[B(\underline{\mathbf{x}},t)]). \quad (6)$$

The choice of the internal heat generation rate in the form given by (5) allows for bioheat heat transfer problems to be considered here. It may be used to model heat transfer via blood perfusion in biological tissues (see, for example, Zhou, Zhang and Chen, 2009). For the problem here, the medium of heat conduction is assumed to be nonhomogeneous such that the thermal conductivity κ, the specific heat capacity c and the density ρ may be given by suitably prescribed functions of $\underline{\mathbf{x}}$. The phase lags τ_q and τ_T of the heat flux components are taken to be constants here.

3 Initial-boundary value problem

Let R be the region in which the partial differential equation in (6) holds. With reference to a Cartesian coordinate system denoted by $Oxyz$, the geometry of R is symmetrical about the z-axis, that is, R and its boundary S can be obtained by rotating respectively a two-dimensional region and a curve by an angle of 360° about the z-axis. On the rz plane, the two-dimensional region and the curve are denoted by Ω and Γ respectively. Fig. 1 gives a sketch of Ω (shaded region) and Γ. In Fig. 1, Γ is shown as an open curve having endpoints A and B on the z-axis. In general, Γ may however also be a closed curve, as in, for example, the case in which R is the hollow cylindrical region defined by $u < r < v$, $0 < z < w$, where u, v and w are positive constants.

If r and θ denote the polar coodinates defined by $x = r\cos\theta$ and $y = r\sin\theta$, the temperature T, the thermal conductivity κ, the specific heat capacity c, the density

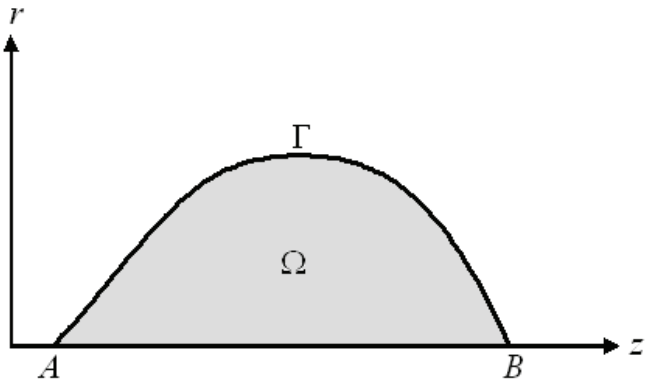

Figure 1: A geometrical sketch of Ω and Γ

ρ and the coefficients A and B in the internal heat source generation rate are assumed here to be functions of r and z only (independent of θ). Thus, $\underline{\mathbf{x}}$ is taken to be given by (r,z) here, where (r,z) refers to a point in $\Omega \cup \Gamma$ (on the rz plane).

The temperature $T(\underline{\mathbf{x}},t)$ and the heat flux vector $\underline{\mathbf{q}}(\underline{\mathbf{x}},t)$ are determined by solving (6) together with (2) for $\underline{\mathbf{x}} \in \Omega$ and $t > 0$ subject to the initial-boundary conditions

$$T(\underline{\mathbf{x}},0) = f_0(\underline{\mathbf{x}}) \text{ and } \frac{\partial}{\partial t}[T(\underline{\mathbf{x}},t)]\bigg|_{t=0} = f_1(\underline{\mathbf{x}}) \text{ for } \underline{\mathbf{x}} \in \Omega \cup \Gamma,$$

$$\underline{\mathbf{q}}(\underline{\mathbf{x}},0) = \underline{\mathbf{q}}_0(\underline{\mathbf{x}}) \text{ for } \underline{\mathbf{x}} \in \Omega \cup \Gamma,$$

$$T(\underline{\mathbf{x}},t) = g_0(\underline{\mathbf{x}},t) \text{ for } \underline{\mathbf{x}} \in \Gamma_1 \textit{ and } t > 0,$$

$$q(\underline{\mathbf{x}},t) = g_1(\underline{\mathbf{x}},t) + g_2(\underline{\mathbf{x}})T(\underline{\mathbf{x}},t) \text{ for } \underline{\mathbf{x}} \in \Gamma_2 \text{ and } t > 0, \tag{7}$$

where Γ_1 and Γ_2 are non-intersecting curves such that $\Gamma_1 \cup \Gamma_2 = \Gamma$, $q(\underline{\mathbf{x}},t) = \underline{\mathbf{n}}(\underline{\mathbf{x}}) \bullet \underline{\mathbf{q}}(\underline{\mathbf{x}},t)$ is the component of the flux $\underline{\mathbf{q}}$ in the direction of the vector $\underline{\mathbf{n}}$, $\underline{\mathbf{n}}$ denotes the outward unit normal vector on the boundary Γ and $f_0(\underline{\mathbf{x}})$, $f_1(\underline{\mathbf{x}})$, $q_0(\underline{\mathbf{x}})$, $g_0(\underline{\mathbf{x}},t)$, $g_1(\underline{\mathbf{x}},t)$ and $g_2(\underline{\mathbf{x}})$ are suitably given functions. Note that if $g_2(\underline{\mathbf{x}}) = 0$ for $\underline{\mathbf{x}} \in \Gamma_2$ then the boundary condition on the last line gives the special case in which the heat flux is known on Γ_2.

In Section 4, we recast the governing partial differential equation in (6) as an integro-differential equation. The integro-differential equation can be solved together with the initial-boundary conditions (7) for $T(\underline{\mathbf{x}},t)$ in Ω as well as for the normal flux $q(\underline{\mathbf{x}},t)$ on Γ_1. A dual-reciprocity boundary element method for solving numerically the integro-differential equation in the Laplace transform domain is given in Section 5.

4 Integro-differential equation

To derive a suitable integro-differential equation for the governing partial differential equation in (6), let

$$T(\underline{\mathbf{x}},t)=\frac{1}{\sqrt{\kappa(\underline{\mathbf{x}})}}\psi(\underline{\mathbf{x}},t). \tag{8}$$

Substituition of (8) into (6) yields

$$\nabla^2(\psi(\underline{\mathbf{x}},t)+\tau_T\frac{\partial}{\partial t}[\psi(\underline{\mathbf{x}},t)])=C_2(\underline{\mathbf{x}})\frac{\partial^2}{\partial t^2}[\psi(\underline{\mathbf{x}},t)]+C_1(\underline{\mathbf{x}})\frac{\partial}{\partial t}[\psi(\underline{\mathbf{x}},t)]+C_0(\underline{\mathbf{x}})\psi(\underline{\mathbf{x}},t)$$

$$-\frac{1}{\sqrt{\kappa(\underline{\mathbf{x}})}}\{B(\underline{\mathbf{x}},t)+\tau_q\frac{\partial}{\partial t}[B(\underline{\mathbf{x}},t)]\}, \tag{9}$$

where

$$C_0(\underline{\mathbf{x}})=\frac{\sqrt{\kappa(\underline{\mathbf{x}})}\nabla^2(\sqrt{\kappa(\underline{\mathbf{x}})})-A(\underline{\mathbf{x}})}{\kappa(\underline{\mathbf{x}})},\ C_1(\underline{\mathbf{x}})=\frac{\rho c-\tau_q A(\underline{\mathbf{x}})}{\kappa(\underline{\mathbf{x}})}+\frac{\tau_T}{\sqrt{\kappa(\underline{\mathbf{x}})}}\nabla^2(\sqrt{\kappa(\underline{\mathbf{x}})}),$$

$$C_2(\underline{\mathbf{x}})=\frac{\rho c\tau_q}{\kappa(\underline{\mathbf{x}})}. \tag{10}$$

It is assumed here that $\nabla^2(\sqrt{\kappa(\underline{\mathbf{x}})})$ exists in the solution domain Ω.

From (9), guided by the analysis in Brebbia, Telles and Wrobel (1984), one may derive the integro-differential equation

$$\begin{aligned}
&\gamma(\underline{\mathbf{x}}_0)(\psi(\underline{\mathbf{x}}_0,t)+\tau_T\frac{\partial}{\partial t}[\psi(\underline{\mathbf{x}}_0,t)])\\
&=\iint_\Gamma G_0(\underline{\mathbf{x}};\underline{\mathbf{x}}_0)(C_2(\underline{\mathbf{x}}))\frac{\partial^2}{\partial t^2}[\psi(\underline{\mathbf{x}},t)]\\
&+C_0(\underline{\mathbf{x}})\psi(\underline{\mathbf{x}},t)-\frac{1}{\sqrt{\kappa(\underline{\mathbf{x}})}}\{B(\underline{\mathbf{x}},t)+\tau_q\frac{\partial}{\partial t}[B(\underline{\mathbf{x}},t)]\})rdrdz\\
&+\int_\Gamma(\{\psi(\underline{\mathbf{x}},t)+\tau_T\frac{\partial}{\partial t}[\psi(\underline{\mathbf{x}},t)]\})rds(\underline{\mathbf{x}})\\
&-G_0(\underline{\mathbf{x}};\underline{\mathbf{x}}_0)\frac{\partial}{\partial n}\{\psi(\underline{\mathbf{x}},t)+\tau_T\frac{\partial}{\partial t}[\psi(\underline{\mathbf{x}},t)]\})rds(\underline{\mathbf{x}})\\
&\qquad\qquad\text{for } \underline{\mathbf{x}}_0=(r_0,z_0)\in\Omega\cup\Gamma \text{ and } t\geq 0,
\end{aligned} \tag{11}$$

where $\partial\psi[(\underline{\mathbf{x}},t)]/\partial n$ denotes the outward normal derivative of the function $\psi(\underline{\mathbf{x}},t)$ on the boundary Γ, $\gamma(\underline{\mathbf{x}}_0)=1$ if $\underline{\mathbf{x}}_0$ lies in the interior of Ω, $\gamma(\underline{\mathbf{x}}_0)=1/2$ if $\underline{\mathbf{x}}_0$ lies

on a smooth part of Γ, $ds(\underline{\mathbf{x}})$ denotes the length of an infinitesimal part of the curve Γ, $G_0(\underline{\mathbf{x}};\underline{\mathbf{x}}_0)$ and $G_1(\underline{\mathbf{x}};\underline{\mathbf{x}}_0)$ are given by

$$G_0(\underline{\mathbf{x}};\underline{\mathbf{x}}_0) = -\frac{K(m(\underline{\mathbf{x}};\underline{\mathbf{x}}_0))}{\pi\sqrt{a(\underline{\mathbf{x}};\underline{\mathbf{x}}_0)+b(r;r_0)}},$$

$$G_1(\underline{\mathbf{x}};\underline{\mathbf{x}}_0) = -\frac{1}{\pi\sqrt{a(\underline{\mathbf{x}};\underline{\mathbf{x}}_0)+b(r;r_0)}}$$

$$\times\{\frac{n_r(\underline{\mathbf{x}})}{2r}[\frac{r_0^2-r^2+(z_0-z)^2}{a(\underline{\mathbf{x}};\underline{\mathbf{x}}_0)-b(r;r_0)}E(m(\underline{\mathbf{x}};\underline{\mathbf{x}}_0))-K(m(\underline{\mathbf{x}};\underline{\mathbf{x}}_0))]$$

$$+n_z(\underline{\mathbf{x}})\frac{z_0-z}{a(r,z;r_0,z_0)-b(r;r_0)}E(m(\underline{\mathbf{x}};\underline{\mathbf{x}}_0))\},$$

$$m(\underline{\mathbf{x}};\underline{\mathbf{x}}_0) = \frac{2b(r;r_0)}{a(\underline{\mathbf{x}};\underline{\mathbf{x}}_0)+b(r;r_0)},$$

$$a(\underline{\mathbf{x}};\underline{\mathbf{x}}_0) = r_0^2+r^2+(z_0-z)^2, \quad b(r;r_0) = 2rr_0, \tag{12}$$

$n_r(\underline{\mathbf{x}})$ and $n_z(\underline{\mathbf{x}})$ are respectively the r and z components of the outward unit normal vector $\underline{\mathbf{n}}$ to the boundary Γ at the point $\underline{\mathbf{x}}$ and K and E denote the complete elliptic integrals of the first and second kind respectively defined by (see Abramowitz and Stegun, 1970)

$$K(m) = \int_0^{\pi/2}\frac{d\theta}{\sqrt{1-m\sin^2\theta}}, \quad E(m) = \int_0^{\pi/2}\sqrt{1-m\sin^2\theta}\,d\theta \tag{13}$$

Note that $0 \le m(\underline{\mathbf{x}};\underline{\mathbf{x}}_0) \le 1$.

5 A boundary element procedure

5.1 Integral equation in Laplace transform domain

Applying the Laplace transform with respect to time t $(0 \le t < \infty)$ on both sides of (11) and using the initial conditions in (7), we obtain the integral equation

$$\gamma(\underline{\mathbf{x}}_0)\varphi(\underline{\mathbf{x}}_0,p) = \iint_\Omega G_0(\underline{\mathbf{x}},\underline{\mathbf{x}}_0)[D(\underline{\mathbf{x}},p)\varphi(\underline{\mathbf{x}},p)+F(\underline{\mathbf{x}},p)]rdrdz$$

$$+\int_\Gamma(\varphi(\underline{\mathbf{x}}_0,p)G_1(\underline{\mathbf{x}},\underline{\mathbf{x}}_0)-G_0(\underline{\mathbf{x}},\underline{\mathbf{x}}_0)\frac{\partial}{\partial n}[\varphi(\underline{\mathbf{x}},p)])rds(\underline{\mathbf{x}})$$

for $\underline{\mathbf{x}}_0 \in \Omega \cup \Gamma$ and $p > 0$, (14)

where p is the Laplace transform parameter (assumed to be real here), $\varphi(\underline{\mathbf{x}}, p)$, $D(\underline{\mathbf{x}}, p)$ and $F(\underline{\mathbf{x}}, p)$ are given by

$$\varphi(\underline{\mathbf{x}}, p) = (1 + p\tau_T)\tilde{\psi}(\underline{\mathbf{x}}, p) - \tau_T \sqrt{\kappa(\underline{\mathbf{x}})} f_0(\underline{\mathbf{x}}),$$

$$D(\underline{\mathbf{x}}, p) = \frac{1}{1 + p\tau_T}(p^2 C_2(\underline{\mathbf{x}}) + pC_1(\underline{\mathbf{x}}) + C_0(\underline{\mathbf{x}})),$$

$$F(\underline{\mathbf{x}}, p) = \frac{\tau_T \sqrt{\kappa(\underline{\mathbf{x}})} f_0(\underline{\mathbf{x}})}{1 + p\tau_T}[p^2 C_2(\underline{\mathbf{x}}) + pC_1(\underline{\mathbf{x}}) + C_0(\underline{\mathbf{x}})]$$
$$-\sqrt{\kappa(\underline{\mathbf{x}})}(C_2(\underline{\mathbf{x}})[pf_0(\underline{\mathbf{x}}) + f_1(\underline{\mathbf{x}})] + C_1(\underline{\mathbf{x}}) f_0(\underline{\mathbf{x}}))$$
$$-\frac{1}{\sqrt{\kappa(\underline{\mathbf{x}})}}\{(1 + p\tau_q)\tilde{B}(\underline{\mathbf{x}}, p) - \tau_q B(\underline{\mathbf{x}}, 0)\}, \tag{15}$$

and $\tilde{\psi}(\underline{\mathbf{x}}, p)$ and $\tilde{B}(\underline{\mathbf{x}}, p)$ are the Laplace transform of $\psi(\underline{\mathbf{x}}, t)$ and $B(\underline{\mathbf{x}}, t)$ respectively, that is,

$$\tilde{\psi}(\underline{\mathbf{x}}, p) = \int_0^\infty \psi(\underline{\mathbf{x}}, t) \exp(-pt) dt, \quad \tilde{B}(\underline{\mathbf{x}}, p) = \int_0^\infty B(\underline{\mathbf{x}}, t) \exp(-pt) dt. \tag{16}$$

If we apply the Laplace transform on (2) as well as the boundary conditions in (7), we obtain

$$\varphi(\underline{\mathbf{x}}, p) = P_0(\underline{\mathbf{x}}, p) \text{ for } \underline{\mathbf{x}} \in \Gamma_1,$$

$$\frac{\partial}{\partial n}[\varphi(\underline{\mathbf{x}}, p)] = P_1(\underline{\mathbf{x}}, p) + P_2(\underline{\mathbf{x}}, p)\varphi(\underline{\mathbf{x}}, p) \text{ for } \underline{\mathbf{x}} \in \Gamma_2, \tag{17}$$

where $P_0(\underline{\mathbf{x}}, p)$, $P_1(\underline{\mathbf{x}}, p)$ and $P_2(\underline{\mathbf{x}}, p)$ are given by

$$P_0(\underline{\mathbf{x}}, p) = (1 + p\tau_T)\sqrt{\kappa(\underline{\mathbf{x}})}\tilde{g}_0(\underline{\mathbf{x}}, p) - \tau_T \sqrt{\kappa(\underline{\mathbf{x}})} f_0(\underline{\mathbf{x}})$$

$$P_1(\underline{\mathbf{x}}, p) = \frac{1}{\sqrt{\kappa(\underline{\mathbf{x}})}}[-\frac{1 + p\tau_q}{1 + p\tau_T}\tau_T g_2(\underline{\mathbf{x}}) f_0(\underline{\mathbf{x}}) - (1 + p\tau_q)\tilde{g}_1(\underline{\mathbf{x}}, p) + \tau_q q_0(\underline{\mathbf{x}})]$$

$$P_2(\underline{\mathbf{x}}, p) = \frac{1}{2\kappa(\underline{\mathbf{x}})}\frac{\partial}{\partial n}[\kappa(\underline{\mathbf{x}})] - (\frac{1 + p\tau_q}{1 + p\tau_T})\frac{g_2(\underline{\mathbf{x}})}{\kappa(\underline{\mathbf{x}})} \tag{18}$$

with $\tilde{g}_0(\underline{\mathbf{x}}, p)$ and $\tilde{g}_1(\underline{\mathbf{x}}, p)$being the Laplace transform of $g_0(\underline{\mathbf{x}}, t)$ and $g_1(\underline{\mathbf{x}}, t)$respectively and $q_0(\underline{\mathbf{x}})$ given by $q_0(\underline{\mathbf{x}}) = \underline{\mathbf{n}} \bullet \underline{\mathbf{q}}_0(\underline{\mathbf{x}})$.

In the Laplace transform space, the problem is then to solve the integral equation in (14) for the unknown function $\varphi(\underline{\mathbf{x}}, p)$ subject to the boundary conditions in (17).

5.2 Discretization of boundary integrals

The curve Γ in Fig. 1 is discretized into N straight line elements denoted by $\Gamma^{(1)}$, $\Gamma^{(2)}, \cdots, \Gamma^{(N-1)}$ and $\Gamma^{(N)}$. The starting and ending points of a typical element $\Gamma^{(k)}$ are given by $\underline{\mathbf{x}}^{(k)} = (r^{(k)}, z^{(k)})$ and $\mathbf{x}^{(k+1)} = (r^{(k+1)}, z^{(k+1)})$ respectively. Two points on the element $\Gamma^{(k)}$, denoted by $\mathbf{x}_0^{(k)} = (r_0^{(k)}, z_0^{(k)})$ and $\underline{\mathbf{x}}_0^{(N+k)} = (r_0^{(N+k)}, z_0^{(N+k)})$, are chosen as

$$\underline{\mathbf{x}}_0^{(k)} = \underline{\mathbf{x}}^{(k)} + \tau(\underline{\mathbf{x}}^{(k+1)} - \underline{\mathbf{x}}^{(k)}),$$

$$\underline{\mathbf{x}}_0^{(N+k)} = \underline{\mathbf{x}}^{(k)} + (1-\tau)(\underline{\mathbf{x}}^{(k+1)} - \underline{\mathbf{x}}^{(k)}), \tag{19}$$

where τ is a chosen number such that $0 < \tau < 1/2$.

If the function φ at $\underline{\mathbf{x}}_0^{(k)}$ and $\underline{\mathbf{x}}_0^{(N+k)}$ is denoted by $\varphi^{(k)}(p)$ and $\varphi^{(N+k)}(p)$ respectively, then it can be approximated as

$$\varphi(\underline{\mathbf{x}}, p) = \frac{[s^{(k)}(\underline{\mathbf{x}}) - (1-\tau)\ell^{(k)}]\varphi^{(k)}(p) - [s^{(k)}(\underline{\mathbf{x}}) - \tau\ell^{(k)}]\varphi^{(N+k)}(p)}{(2\tau-1)\ell^{(k)}} \text{ for } \underline{\mathbf{x}} \in \Gamma^{(k)}, \tag{20}$$

where $\ell^{(k)} = s^{(k)}(\underline{\mathbf{x}}^{(k+1)})$ and $s^{(k)}(\underline{\mathbf{x}})$ is the arc length along the element $\Gamma^{(k)}$ as defined by

$$s^{(k)}(\underline{\mathbf{x}}) = \sqrt{(r-r^{(k)})^2 + (z-z^{(k)})^2}. \tag{21}$$

Similarly, if $h(\underline{\mathbf{x}}, p) = \partial\phi(\underline{\mathbf{x}}, p)]/\partial n$ is given by $h^{(k)}(p)$ and $h^{(N+k)}(p)$ at $\underline{\mathbf{x}}_0^{(k)}$ and $\underline{\mathbf{x}}_0^{(N+k)}$ respectively, it can be approximately as

$$h(\underline{\mathbf{x}}, p) = \frac{[s^{(k)}(\underline{\mathbf{x}}) - (1-\tau)\ell^{(k)}]h^{(k)}(p) - [s^{(k)}(\underline{\mathbf{x}}) - \tau\ell^{(k)}]h^{(N+k)}(p)}{(2\tau-1)\ell^{(k)}}$$
$$\text{for } \underline{\mathbf{x}} \in \Gamma^{(k)}. \tag{22}$$

The approximations in (20) and (22) give what are known as discontinuous linear elements in the literature (see, for example, Paris and Canas, 1997).

With (20) and (22), the line integrals in the integral equation in (14) can be approximated as

$$\int_{\Gamma} \phi(\underline{\mathbf{x}}, p) G_1(\underline{\mathbf{x}}, \underline{\mathbf{x}}_0) r ds(\underline{\mathbf{x}})$$
$$= \sum_{k=1}^{N} \frac{1}{(2\tau-1)\ell^{(k)}} \{[-(1-\tau) l^{(k)} I_2^{(k)}(\underline{\mathbf{x}}_0) + I_4^{(k)}(\underline{\mathbf{x}}_0)] \phi^{(k)}(p)$$
$$+ [\tau\, \ell^{(k)} I_2^{(k)}(\underline{\mathbf{x}}_0) - I_4^{(k)}(\underline{\mathbf{x}}_0)] \phi^{(N+k)}(p)\}, \quad (23)$$

and

$$\int_{\Gamma} h(\underline{\mathbf{x}}, p) G_0(\underline{\mathbf{x}}, \underline{\mathbf{x}}_0) r ds(\underline{\mathbf{x}})$$
$$= \sum_{k=1}^{N} \frac{1}{(2\tau-1)\ell^{(k)}} \{[-(1-\tau) l^{(k)} I_1^{(k)}(\underline{\mathbf{x}}_0) + I_3^{(k)}(\underline{\mathbf{x}}_0)] h^{(k)}(p)$$
$$+ [\tau \ell^{(k)} I_1^{(k)}(\underline{\mathbf{x}}_0) - I_3^{(k)}(\underline{\mathbf{x}}_0)] h^{(N+k)}(p)\}, \quad (24)$$

where

$$I_1^{(k)}(\underline{\mathbf{x}}_0) = \int_{\Gamma^{(k)}} G_0(\underline{\mathbf{x}}, \underline{\mathbf{x}}_0) r ds(\underline{\mathbf{x}}) \quad I_2^{(k)}(\underline{\mathbf{x}}_0) = \int_{\Gamma^{(k)}} G_1(\underline{\mathbf{x}}, \underline{\mathbf{x}}_0) r ds(\underline{\mathbf{x}})$$

$$I_3^{(k)}(\underline{\mathbf{x}}_0) = \int_{\Gamma^{(k)}} s(\underline{\mathbf{x}}) G_0(\underline{\mathbf{x}}, \underline{\mathbf{x}}_0) r ds(\underline{\mathbf{x}}) \quad I_4^{(k)}(\underline{\mathbf{x}}_0) = \int_{\Gamma^{(k)}} s(\underline{\mathbf{x}}) G_1(\underline{\mathbf{x}}, \underline{\mathbf{x}}_0) r ds(\underline{\mathbf{x}}) \quad (25)$$

The integrals over $\Gamma^{(k)}$ in (25) can be evaluated using numerical integration formulae such as the Gaussian quadratures given in Abramowitz and Stegun (1970).

5.3 Dual-reciprocity approximation of domain integral

The dual-reciprocity method can be used to approximate the domain integral over the domain Ω in (14) (see, for example, Patridge, Brebbia and Wrobel, 1992). The method requires L well-spaced out collocation points to be chosen in the interior of the domain Ω. These points are denoted by $\underline{\mathbf{x}}_0^{(2N+1)}$, $\underline{\mathbf{x}}_0^{(2N+2)}$, $\cdots$, $\underline{\mathbf{x}}_0^{(2N+L-1)}$ and $\underline{\mathbf{x}}_0^{(2N+L)}$. Besides the L interior points, the points $\underline{\mathbf{x}}_0^{(k)}$ and $\underline{\mathbf{x}}_0^{(N+k)}$ on the element $\Gamma^{(k)}$ ($k = 1, 2, \cdots, N$) are also used as collocation points. Thus, there are $2N+L$ collocation points.

The domain integral is approximated as

$$\iint_{\Omega} G_0(\underline{\mathbf{x}},\underline{\mathbf{x}}_0)[D(\underline{\mathbf{x}},p)\phi(\underline{\mathbf{x}},p)+F(\underline{\mathbf{x}},p)]rdrdz$$
$$= \sum_{k=1}^{2N+L}[D(\underline{\mathbf{x}}_0^{(k)},p)\phi^{(k)}(p)+F(\underline{\mathbf{x}}_0^{(k)},p)]\sum_{j=1}^{2N+L}W^{(kj)}\Psi^{(j)}(\underline{\mathbf{x}}), \quad (26)$$

where $\phi^{(k)}(p)=\phi(\underline{\mathbf{x}}_0^{(k)},p)$ for $k=1,\ 2,\ \cdots,\ 2N+\ L$, the coefficients $W^{(kj)}$ are defined implicitly by

$$\sum_{j=1}^{2N+L}W^{(kj)}\phi^{(n)}(\underline{\mathbf{x}}_0^j)=\begin{cases}0 & \text{if } n\neq k\\ 1 & \text{if } n=k\end{cases} \text{ for } n,k=1,2,\ldots,2N+L, \quad (27)$$

the function $\Psi^{(j)}(\underline{\mathbf{x}})$ is expressed in terms of line integrals over Γ as

$$\Psi^{(j)}(\underline{\mathbf{x}}_0)=\gamma(\underline{\mathbf{x}}_0)\chi^{(j)}(\underline{\mathbf{x}}_0)+\int_{\Gamma} rG_0(\underline{\mathbf{x}},\underline{\mathbf{x}}_0)\frac{\partial}{\partial n}[\chi^{(j)}(\underline{\mathbf{x}})]ds(\underline{\mathbf{x}})$$
$$-\int_{\Gamma} r\chi^{(j)}(\underline{\mathbf{x}})G_1(\underline{\mathbf{x}},\underline{\mathbf{x}}_0)]ds(\underline{\mathbf{x}}) \text{ for } j=1,2,\ldots,2N+L, \quad (28)$$

the functions $\phi^{(n)}$ and $\chi^{(n)}$ are local interpolating functions centered about the collocation point $\underline{\mathbf{x}}_0^{(n)}$ and chosen to satisfy the partial differential equation

$$\frac{\partial^2}{\partial r^2}[\chi^{(n)}(\underline{\mathbf{x}})]+\frac{1}{r}\frac{\partial}{\partial r}[\chi^{(n)}(\underline{\mathbf{x}})]+\frac{\partial^2}{\partial z^2}[\chi^{(n)}(\underline{\mathbf{x}})]=\phi^{(n)}(\underline{\mathbf{x}}). \quad (29)$$

In earlier works such as Patridge, Brebbia and Wrobel (1992), $\phi^{(n)}$ and $\chi^{(n)}$ are taken to be of the form

$$\phi^{(n)}(\underline{\mathbf{x}})=[\frac{4}{3}-\frac{r_0^{(n)}}{3r}]\sigma(\underline{\mathbf{x}};\underline{\mathbf{x}}_0^{(n)}),\chi^{(n)}(\underline{\mathbf{x}})=\frac{1}{9}[\sigma(\underline{\mathbf{x}};\underline{\mathbf{x}}_0^{(n)})]^3, \quad (30)$$

where $\sigma(\underline{\mathbf{x}};\underline{\mathbf{x}}_0^{(n)})$ is the distance between the points $\underline{\mathbf{x}}$ and $\underline{\mathbf{x}}_0^{(n)}$ on the rz plane, that is

$$\sigma(\underline{\mathbf{x}};\underline{\mathbf{x}}_0^{(n)})=\sqrt{(r-r_0^{(n)})^2+(z-z_0^{(n)})^2}. \quad (31)$$

Although the interpolating functions in (30) are simple in form, there is a singularity in the function $\phi^{(n)}(\underline{\mathbf{x}})$ at $r=0$. This may pose a problem if $r=0$ is a part

of the boundary of the solution domain Ω. To remove the singularity, in Wang, Mattheij and ter Morsche (2003), the interpolating functions are constructed from the integrals

$$\phi^{(}n)(\underline{\mathbf{x}}) = \int_0^{2\pi} \left((r\cos\theta - r_0^{(n)})^2 + r^2\sin\theta + (z - z_0^{(n)})^2 \right)^{1/2} d\theta$$

$$\chi^{(}n)(\underline{\mathbf{x}}) = \frac{1}{12}\int_0^{2\pi} ((r\cos\theta - r_0^{(n)})^2 + r^2\sin^2\theta + (z - z_0^{(n)})^2)^{3/2} d\theta. \tag{32}$$

The formulae in (32), however, give rise to interpolating functions which are quite complicated in form and expressed in terms of special functions such as the elliptic integrals. We will not go into the details here.

To use relatively simple interpolating functions which are bounded in the solution domain Ω, we modify $\chi^{(n)}(\underline{\mathbf{x}})$ in (30) to take the form

$$\chi^{(n)}(\underline{\mathbf{x}}) = \frac{1}{9}\{[\sigma(r,z;r_0^{(n)},z_0^{(n)})]^3 + [\sigma(r,z;-r_0^{(n)},z_0^{(n)})]^3\}. \tag{33}$$

Consequently, from (29), $\phi^{(n)}(\underline{\mathbf{x}})$ is given by

$$\phi^{(n)}(\underline{\mathbf{x}}) = [\frac{4}{3} - \frac{r_0^{(n)}}{3r}]\sigma(r,z;r_0^{(n)},z_0^{(n)}) + [\frac{4}{3} + \frac{r_0^{(n)}}{3r}]\sigma(r,z;-r_0^{(n)},z_0^{(n)}). \tag{34}$$

As required, the function $\phi^{(n)}(\underline{\mathbf{x}})$ in (34) tends to a finite number as r tends to zero. Note that the point $(-r_0^{(n)},z_0^{(n)})$ may be regarded as the virtual mirror image of $(r_0^{(n)},z_0^{(n)})$ about the r axis in Fig. 1. The interpolating functions in (33) and (34) appear to have been first proposed in Yun and Ang (2010). For specific test problems solved by the axisymmetric dual-reciprocity boundary element method, such interpolating functions are found to deliver numerical solutions which are comparable in accuracy to those given by the more complicated functions given by (32).

5.4 System of linear algebraic equations

From (23), (24) and (26), the integral differential equation in (14) can be approximated as

$$\gamma(\underline{\mathbf{x}}_0^{(m)})\phi^{(m)}p) = \sum_{k=1}^{2N+L} [D(\underline{\mathbf{x}}^{(k)},p)\phi^{(k)}(p) + F(\underline{\mathbf{x}}^{(k)},p)]\mu^{(km)}$$

$$+\sum_{k=1}^{N}\frac{1}{(2\tau-1)\ell^{(k)}}\{[-(1-\tau)l^{(k)}I_2^{(k)}(\underline{\mathbf{x}}^{(m)})+I_4^{(k)}(\underline{\mathbf{x}}^{(m)})]\phi^{(k)}(p)$$
$$+[\tau\ell^{(k)}I_2^{(k)}(\underline{\mathbf{x}}^{(m)})-I_4^{(k)}(\underline{\mathbf{x}}^{(m)})]\phi^{(N+k)}(p)-[-(1-\tau)\ell^{(k)}I_1^{(k)}(\underline{\mathbf{x}}^{(m)})+I_3^{(k)}(\underline{\mathbf{x}}^{(m)})]h^{(k)}(p)$$
$$-[\tau\ell^{(k)}I_1^{(k)}(\underline{\mathbf{x}}^{(m)})-I_3^{(k)}(\underline{\mathbf{x}}^{(m)})]h^{(N+k)}(p)\}\ \text{for}\ m=1,2,\cdots,2N+L, \tag{35}$$

where $\mu^{(km)}$ is given by

$$\mu^{(km)}=\sum_{j=1}^{2N+L}W^{(kj)}\Psi^{(j)}(\underline{\mathbf{x}}^{(m)}). \tag{36}$$

The boundary conditions in (17) can be applied in (35) to obtain

$$\gamma(\underline{\mathbf{x}}_0^{(m)})\{\alpha^{(m)}\phi^{(m)}(p)+\beta^{(m)}R^{(m)}(p)\}$$
$$=\sum_{k=1}^{2N+L}[D(\underline{\mathbf{x}}_0^{(k)},p)(\alpha^{(k)}\phi^{(k)}(p)+\beta^{(k)}R^{(k)}(p))+F(\underline{\mathbf{x}}_0^{(k)},p)]\mu^{(km)}$$
$$+\sum_{k=1}^{N}\frac{1}{(2\tau-1)\ell^{(k)}}\{[-(1-\tau)l^{(k)}I_2^{(k)}(\underline{\mathbf{x}}_0^{(m)})+I_4^{(k)}(\underline{\mathbf{x}}_0^{(m)})]$$
$$-\alpha^{(k)}P_2^{(k)}(p)(-(1-\tau)\ell^{(k)}I_1^{(k)}(\underline{\mathbf{x}}_0^{(m)})+I_3^{(k)}(\underline{\mathbf{x}}_0^{(m)}))](\alpha^{(k)}\phi^{(k)}(p)+\beta^{(k)}R^{(k)}(p))$$
$$+[\tau\ell^{(k)}I_2^{(k)}(\underline{\mathbf{x}}_0^{(m)})-I_4^{(k)}(\underline{\mathbf{x}}_0^{(m)})-\alpha^{(N+k)}P_2^{(N+k)}(p)(\tau\ell^{(k)}I_1^{(k)}(\underline{\mathbf{x}}_0^{(m)})-I_3^{(k)}(\underline{\mathbf{x}}_0^{(m)}))]$$
$$\times(\alpha^{(N+k)}\phi^{(N+k)}(p)+\beta^{(N+k)}R^{(N+k)}(p))$$
$$-[-(1-\tau)\ell^{(k)}I_1^{(k)}(\underline{\mathbf{x}}_0^{(m)})+I_3^{(k)}(\underline{\mathbf{x}}_0^{(m)})][\alpha^{(k)}P_1^{(k)}(p)+\beta^{(k)}h^{(k)}(p)]$$
$$-[\tau\ell^{(k)}I_1^{(k)}(\underline{\mathbf{x}}_0^{(m)})-I_3^{(k)}(\underline{\mathbf{x}}_0^{(m)})][\alpha^{(N+k)}P_1^{(N+k)}(p)+\beta^{(N+k)}h^{(N+k)}(p)]\}$$
$$\text{for}\ m=1,2,\cdots,2N+L, \tag{37}$$

where $R^{(m)}(p)$, $\alpha^{(m)}$, $\beta^{(m)}$, $P_1^{(n)}$, and $P_2^{(n)}$ (for $m=1,2,\cdots,2N+L$ and $n=1,2,\cdots,N,N+1,\cdots,2N-1,2N$) are defined by

$$\alpha^{(m)}=\begin{cases}0 & \text{if } \underline{\mathbf{x}}_0^{(m)} \text{ lies on a boundary element where } \phi \text{ is known,}\\ 1 & \text{otherwise,}\end{cases}$$

$$\beta^{(m)}=1-\alpha^{(m)},R^{(m)}(p)=P_0(\underline{\mathbf{x}}_0^{(m)},p),P_1^{(n)}=P_1(\underline{\mathbf{x}}_0^{(n)},p),P_2^{(n)}=P_2(\underline{\mathbf{x}}_0^{(n)},p). \tag{38}$$

Note that the functions $P_1(\underline{\mathbf{x}}^{(n)},p)$ and $P_2(\underline{\mathbf{x}}^{(n)},p)$ are defined only for the collocation point $\underline{\mathbf{x}}^{(n)}$ which lies on a boundary element where ϕ is not known. Thus, in

(37), the coefficient $\alpha^{(n)}$ is always multiplied to $P_1^{(n)}$ and $P_2^{(n)}$. Likewise, $\beta^{(m)}$ is always multiplied to $R^{(m)}(p)$ since $P_0(\underline{\mathbf{x}}_0^{(m)}, p)$ is defined only for $\underline{\mathbf{x}}_0^{(m)}$ which lies on a boundary element where ϕ is known.

The system (37) comprises $2N+L$ linear algebraic equations in $2N+L$ unknowns. The unknowns are $\phi^{(2N+n)}(p)$ for $n = 1, 2, \cdots, L$, $\phi^{(k)}(p)$ if ϕ is not known on the boundary element $\Gamma^{(k)}$, and $h^{(k)}(p)$ if ϕ is known on the boundary element $\Gamma^{(k)}$.

5.5 Inversion of Laplace transform solution

Once $\phi(\underline{\mathbf{x}}, p)$ is determined, the Laplace transform of $\psi(\underline{\mathbf{x}}, t)$, that is, $\tilde{\psi}(\underline{\mathbf{x}}, p)$, can be evaluated from (15). The temperature $T(\underline{\mathbf{x}}, t)$ can then be recovered by inverting $\tilde{\psi}(\underline{\mathbf{x}}, p)/\sqrt{\kappa(\underline{\mathbf{x}})}$ by using a numerical technique. A survey and comparison of some numerical Laplace transform inversion methods may be found in Davies and Martin (1979). For the numerical inversion of the Laplace transform here, the numerical method due to Stehfest (1970) is used here.

Using the Stehfest's algorithm, we obtain the approximation:

$$T(\underline{\mathbf{x}}, t) \approx \frac{\ln(2)}{t} \sum_{n=1}^{2M} V_n \frac{1}{\sqrt{\kappa(\underline{\mathbf{x}})}} \tilde{\psi}(\underline{\mathbf{x}}, \frac{n \ln(2)}{t}) \tag{39}$$

where M is a positive integer and

$$V_n = (-1)^{n+M} \sum_{m=[(n+1)/2]}^{\min(n,M)} \frac{m^M (2m)!}{(M-m)!m!(m-1)!(n-m)!(2m-n)!}, \tag{40}$$

where $[r]$ denotes the integer part of the real number r.

Similarly, once $h(\underline{\mathbf{x}}, p)$ is known at all points on the boundary Γ, the Laplace transform of the normal flux across the boundary, that is, $\tilde{q}(\underline{\mathbf{x}}, p)$, can be determined from

$$h(\underline{\mathbf{x}}, p) = \frac{1}{\sqrt{\kappa(\underline{\mathbf{x}})}} [-(1 + p\tau_q)\tilde{q}(\underline{\mathbf{x}}, p) + \tau_q q_0(\underline{\mathbf{x}})] + \frac{1}{2\kappa(\underline{\mathbf{x}})} \frac{\partial}{\partial n} [\kappa(\underline{\mathbf{x}})], \tag{41}$$

and the Stehfest's formula can be used to invert $\tilde{q}(\underline{\mathbf{x}}, p)$ to obtain the normal flux $q(\underline{\mathbf{x}}, t)$.

6 Specific problems

In this section, the Laplace transform dual-reciprocity boundary element method presented above is used to solve some specific problems. The first three problems

are initial-boundary value problems which have known exact solutions. They are specially designed to test the validity of the method as well as to assess its accuracy. In the last problem, the method is applied to simulate the axisymmetric dual-phase-lag heat conduction in a particular exponentially graded cylindrical solid. The effects of the phase lags and the spatial variations of the thermal properties on the temperature distribution are examined.

Problem 1. For a test problem, take the solution domain as $0 < r < 1$, $0 < z < 1$ (a solid cylinder). The coefficient κ, ρ, c, τ_T and τ_q are given by $\kappa = 1+z$, $\rho c = 1$, $\tau_T = 1/10$ and $\tau_q = 1/5$. The internal heat generation term Q is given by

$$Q(\underline{\mathbf{x}},t) = -T(\underline{\mathbf{x}},t) - \frac{9}{4}(3+4z)\exp(-t).$$

The initial-boundary conditions are given by

$$T(\underline{\mathbf{x}},0) = r^2+z^2 \text{ for } 0 < r < 1, 0 < z < 1,$$

$$\frac{\partial}{\partial t}[T(\underline{\mathbf{x}},t)]\bigg|_{t=0} = -(r^2+z^2) \text{ for } 0 < r < 1, 0 < z < 1,$$

$$T(1,z,t) = (1+z^2)\exp(-t) \text{ for } 0 < z < 1, t > 0,$$

$$\underline{\mathbf{q}}(\underline{\mathbf{x}},0) = -\frac{9}{4}r(1+z)\underline{\mathbf{e}}_r - \frac{9}{4}(z^2+z)\underline{\mathbf{e}}_z \text{ for } 0 < r < 1, 0 < z < 1,$$

$$q(r,0,t) = 0 \text{ for } 0 < r < 1, t > 0,$$

$$q(r,1,t) = -\frac{9}{2}\exp(-t) \text{ for } 0 < r < 1, t > 0,$$

where $\underline{\mathbf{e}}_r$ and $\underline{\mathbf{e}}_z$ are unit magnitude vectors pointing in the positive direction of the r and z axes respectively.

From (17), in the Laplace transform space, the problem is to determine $\phi(\underline{\mathbf{x}},p)$ which satisfies the boundary conditions

$$\phi(1,z,p)=\sqrt{1+z}(1+z^2)[\frac{1+\frac{1}{10}p}{1+p}-\frac{1}{10}] \text{ for } 0<z<1,\ p>0,$$

$$\frac{\partial}{\partial n}[\phi(\underline{\mathbf{x}},p)]\Big|_{z=0}=-\frac{1}{10}r^2\frac{1+\frac{1}{5}p}{1+\frac{1}{10}p}+r^2\frac{1+\frac{1}{5}p}{1+p}$$

$$+(-\frac{1}{2}-\frac{1+\frac{1}{5}p}{1+\frac{1}{10}p})\phi(r,0,p) \quad \text{for } 0<r<1,\ p>0,$$

and

$$\frac{\partial}{\partial n}[\phi(\underline{\mathbf{x}},p)]\Big|_{z=1}=\frac{1}{\sqrt{2}}[-\frac{1}{10}(r^2+1)\frac{1+\frac{1}{5}p}{1+\frac{1}{10}p}$$

$$+\frac{1+\frac{1}{5}p}{1+p}(r^2+\frac{11}{2})-\frac{9}{10}]+(\frac{1}{4}-\frac{1+\frac{1}{5}p}{2(1+\frac{1}{10}p)})\phi(r,1,p) \text{for } 0<r<1,\ p>0.$$

For the specific problem here, the boundary Γ comprises three equal length straight lines. Each of the straight lines is divided into N_0 equal length elements, so that the total number of elements is $3N_0$, that is, $N=3N_0$. The interior collocation points are taken to be given by $(i/(L_0+1), j/(L_0+1))$ for $i,j=1,\ 2,\ \cdots, L_0$, that is, the total number of interior collocation points is given by L_0^2. In the approximate formula (39) for inverting Laplace transformation, we take $M=4$.

In Table 1, numerical values of the temperature at $t=0.10$, obtained using $(N_0,L_0)=(10,3)$ (Set A) and $(N_0,L_0)=(40,15)$ (Set B), are compared with the exact solution of the test problem given by $T(r,z,t)=(r^2+z^2)\exp(-t)$.

The numerical values in Set B are significantly more accurate than those in Set A. Thus, the numerical solution converges to the exact one when the calculation is refined by using more elements and collocation points.

The numerical temperature at $(r,z)=(0.50,0.50)$, obtained using $N_0=10$ and $L_0=3$, is compared graphically with the exact temperature over the time period $0<t<2$ in Fig. 2. The graphs for the numerical and the exact temperature are almost visually indistinguishable.

Table 1: Numerical and exact values of $T\ (r,z,0.10)$.

(r,z)	Set A	Set B	Exact
(0.25,0.25)	0.11832	0.11312	0.11310
(0.50,0.25)	0.28338	0.28278	0.28276
(0.75,0.25)	0.56613	0.56554	0.56552
(0.25,0.50)	0.28312	0.28277	0.28276
(0.50,0.50)	0.45269	0.45243	0.45242
(0.75,0.50)	0.73547	0.73519	0.73518
(0.25,0.75)	0.56572	0.56553	0.56552
(0.50,0.75)	0.73535	0.73519	0.73518
(0.75,0.75)	1.01813	1.01795	1.01794

For the initial-boundary conditions here, the temperature is specified at $r = 1$ for $t > 0$. Thus, it may be of interest to find out if the normal flux across $r = 1$ can be accurately recovered by the dual-reciprocity boundary element procedure. In Fig. 3, we plot the numerical and the exact flux $\mathbf{q}(\underline{\mathbf{x}},t) \bullet \underline{\mathbf{e}}_r$ at time $t = 0.10$ against $0 < z < 1$ on the boundary $r = 1$. There is a good agreement between the numerical and the exact flux. The numerical values of the normal flux in Fig. 3 are computed using $N_0 = 10$ and $L_0 = 3$. The percentage errors in the numerical values are less than 0.20%.

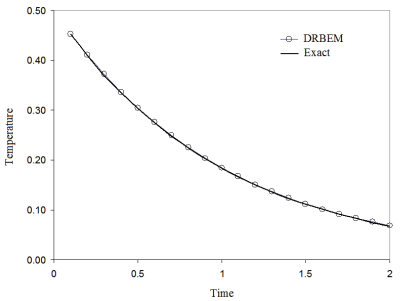

Figure 2: A graphical comparison of the numerical and exact temperature.

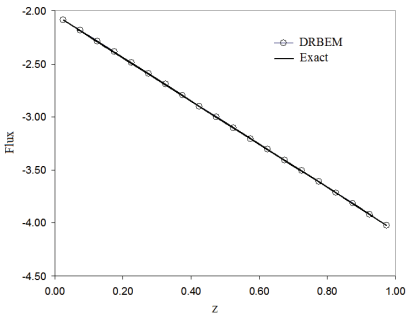

Figure 3: A graphical comparison of the numerical and exact normal flux.

Problem 2. Consider a hollow cylinder occupying the region $1 < r < 2$, $1 < z < 2$. The values of ρc, τ_T and τ_q are respectively taken to be 1, 1/10 and 1/5. The thermal conductivity of the hollow cylinder is set as $\kappa = r + z$ and the internal heat

generation is given by

$$Q(\underline{\mathbf{x}},t) = -\frac{51}{52}(5r+6z)\sin(t) + (\frac{5}{52}(5r+6z) + (\frac{1}{2}r^2+z^2))\cos(t).$$

The initial conditions are given by

$$T(\underline{\mathbf{x}},0) = 0 \text{ for } 1<r<2,\ 1<z<2,$$

$$\frac{\partial}{\partial t}[T(\underline{\mathbf{x}},t)]\Big|_{t=0} = \frac{1}{2}r^2+z^2 \text{ for } 1<r<2,\ 1<z<2,$$

$$\underline{\mathbf{q}}(\underline{\mathbf{x}},0) = \frac{5}{52}r(r+z)\underline{\mathbf{e}}_r + \frac{5}{26}z(r+z)\underline{\mathbf{e}}_z \text{ for } 1<r<2,\ 1<z<2,$$

and the boundary conditions by

$$T(1,z,t) = (\frac{1}{2}+z^2)\sin(t) \text{ for } 1<z<2,\ t>0,$$

$$T(2,z,t) = (2+z^2)\sin(t) \text{ for } 1<z<2,\ t>0,$$

$$q(r,1,t) = \frac{51}{26}(r+1)\sin(t) - \frac{5}{26}(r+1)\cos(t) \text{ for } 1<r<2,\ t>0,$$

$$q(r,2,t) = -\frac{51}{13}(r+2)\sin(t) + \frac{5}{13}(r+2)\cos(t) \text{ for } 1<r<2,\ t>0.$$

In the Laplace transform space, the initial-boundary conditions give

$$\phi(1,z,p) = \sqrt{1+z}\frac{1+\frac{1}{10}p}{1+p^2}(\frac{1}{2}+z^2) \text{ for } 1<z<2,\ p>0,$$

$$\phi(2,z,p) = \sqrt{2+z}\frac{1+\frac{1}{10}p}{1+p^2}(2+z^2) \text{ for } 1<z<2,\ p>0,$$

$$\frac{\partial}{\partial n}[\phi(\underline{\mathbf{x}},p)]\Big|_{z=1} = \frac{1}{\sqrt{r+1}}[-\frac{1+\frac{1}{5}p}{1+p^2}(\frac{51}{26}(r+1)$$

$$-\frac{5}{26}(r+1)p-(\frac{1}{2}r^2+1))-\frac{1}{26}(r+1)]$$

$$+\frac{1}{r+1}(-\frac{1}{2}-\frac{1+\frac{1}{5}p}{1+\frac{1}{10}p})\phi(r,1,p) \quad \text{for } 1<r<2,\ p>0,$$

and

$$\frac{\partial}{\partial n}[\phi(\underline{\mathbf{x}},p)]\Big|_{z=2} = \frac{1}{\sqrt{r+2}}[-\frac{1+\frac{1}{5}p}{1+p^2}(-\frac{51}{13}(r+2)+\frac{5}{13}(r+2)p-(\frac{1}{2}r^2+4))$$

$$+\frac{1}{13}(r+2)]+\frac{1}{r+2}(\frac{1}{2}-\frac{1+\frac{1}{5}p}{1+\frac{1}{10}p})\phi(r,2,p) \quad \text{for } 1<r<2,\ p>0.$$

As this test problem involves the sinusoidal functions $\sin(t)$ and $\cos(t)$ in the heat generation term and the initial boundary conditions, it may be of interest to see if the numerical solution can be recovered properly within one period of the sinusoidal functions, that is, within the time interval $0 \le t \le 2\pi$. To obtain some numerical results, the boundary Γ is discretized into 160 elements, 225 well spaced interior points are selected to be interior collocation points, the parameter τ in the discontinuous elements is taken to be 0.25, and $M = 11$ is used in the numerical Laplace transform inversion formula. At the points $(1.25, 1.25)$, $(1.50, 1.50)$ and $(1.75, 1.75)$, the numerical and the exact temperature and are plotted against time t for $0 \le t \le 2\pi$ in Fig. 4. The exact solution given by $T(r,z,t) = (\frac{1}{2}r^2+z^2)\sin(t)$ is plotted using thick solid lines for all the three points. It appears that temperature can be properly recovered over the time period $0 \le t \le 2\pi$ by the boundary element procedure in Section 5. On the whole, the numerical values of T seem to be more accurate at lower time t. There is a slight deterioration in the accuracy of the numerical temperature near $t = 2\pi$. More terms may be required in the numerical Laplace transform formula to achieve the same level of accuracy for larger t.

Problem 3. Take the solution domain to be the hemispherical in shape given by $r^2+z^2<1$, $0<z<1$. The values of phase lags τ_T and τ_q are taken to be $1/10$

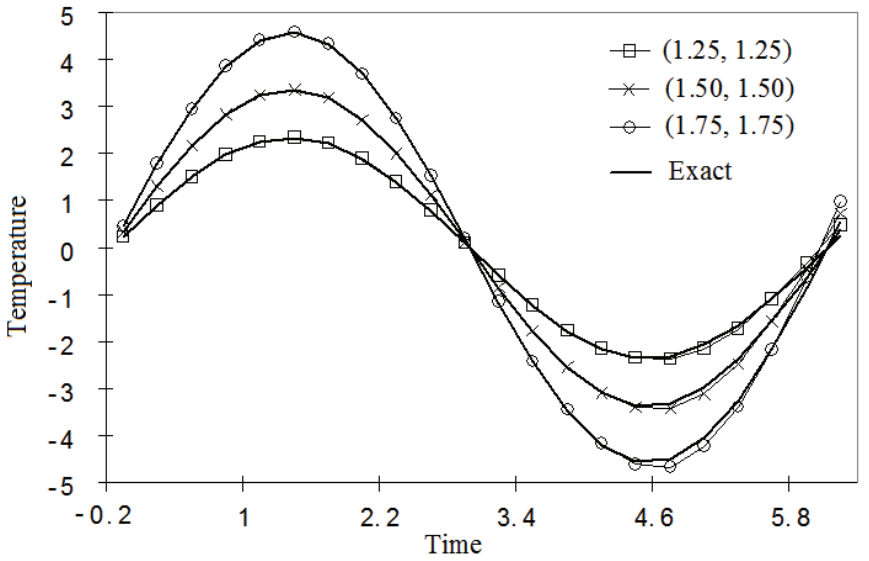

Figure 4: A graphical comparison of the numerical and exact temperature at the points (1.25, 1,25), (1.50, 1.50) and (1.75, 1.75) over a period of time. The exact solution at each point is plotted using a thick solid line.

and $1/5$ respectively. The thermal conductivity κ and heat capacity c vary spatially exponentially as $\kappa = \kappa_0 \exp(\sigma z)$ and $c = c_0 \exp(\sigma z)$ with $\kappa_0 = c_0 = \sigma = 1$. The density is taken to be $\rho = \rho_0 = 1$ and the internal heat generation by

$$Q(\underline{\mathbf{x}},t) = \frac{5}{4}((2+\frac{14}{5}r^2)\sin(2z) - \frac{9}{5}(2+r^2)\cos(2z))\exp(z-t).$$

The initial-boundary conditions are given by

$$T(\underline{\mathbf{x}},0) = (2+r^2)\sin(2z) \text{ for } 0 < r < 1, 0 < z < 1,$$

$$\frac{\partial}{\partial t}[T(\underline{\mathbf{x}},t)]\Big|_{t=0} = -(2+r^2)\sin(2z) \text{ for } 0 < r < 1, 0 < z < 1,$$

$$\underline{\mathbf{q}}(\underline{\mathbf{x}},0) = -\frac{9}{4}\exp(z)(r\sin(2z)\underline{\mathbf{e}}_r + (2+r^2)\cos(2z)\underline{\mathbf{e}}_z) \text{ for } 0 < r < 1, 0 < z < 1,$$

$T(r,0,t) = 0$ for $0 < r < 1, t > 0$,

$T(r,z,t) = (3-z^2)\sin(2z)\exp(-t)$ for $r^2+z^2 = 1,\ 0 < r < 1,\ 0 < z < 1, t > 0$.

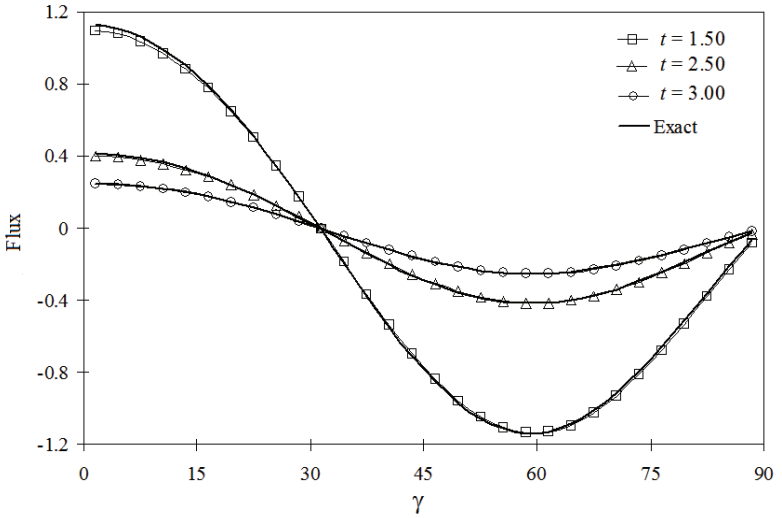

Figure 5: A graphical comparison of the numerical and exact normal flux across the boundary $r^2+z^2 = 1,\ 0 < r < 1,\ 0 < z < 1$ at time $t = 1.50$, 2.50 and 3.0.

For the numerical solution, the boundary is discretized into 60 elements and 37 well spaced collocation points are selected in the interior of the solution domain. For the Stehfest's algorithm in (39), M is chosen to be 8. The normal flux of the temperature is not specified in the boundary conditions. Thus, the numerical normal flux on the circular part of the boundary ($r^2+z^2 = 1$) is compared with exact normal flux given by

$$q(r,z,t) = -\frac{9}{4}\exp(z-t)(r^2\sin(2z)+(2+r^2)z\cos(2z)) \text{ for } r^2+z^2 = 1,\ 0 < r < 1,\ 0 < z < 1.$$

Note that the exact solution of the problem under consideration here is $T(r,z,t) = (2+r^2)\sin(2z)\exp(-t)$.

Fig. 5 gives a graphical comparison of the numerical and exact normal flux on $r^2+z^2=1$, $0<r<1$, $0<z<1$ at time $t=1.50$, 2.50 and 3.0. The normal flux is plotted against γ which is defined by $\gamma=(180/\pi)\arctan(r/z)$. On the whole, there is a reasonably good agreement between the numerical and exact normal flux. Perhaps, as may be expected, the numerical values of the flux have been observed to be slightly less accurate at points very near the sharp corners $(r,z)=(0,1)$ and $(r,z)=(1,0)$ of the solution domain (where γ is given by 0 and 90 respectively).

Problem 4. Consider now the heating of a nonhomogeneous material which occupies the cylindrical region $0<r<a$, $0<z<a$, where a is a positive constant. The thermal conductivity κ, density ρ and specific heat c of the materials are assumed to vary exponentially in the z direction according to $\kappa=\kappa_0\exp(\sigma z)$ and $\rho c=\rho_0 c_0\exp(\sigma z)$, where σ is a constant. The center of the surface $z=0$ of the cylinder is subject to a uniform heat flux q_0 over a small region of radius of $r_c<a$. Mathematically, the problem is to solve (6) with $A=0$ and $B=0$ (that is, with no internal heat generation) inside the cylindrical region $0<r<a$, $0<z<a$, subject to the initial conditions

$$T(\underline{\mathbf{x}},0)=T_0 \text{ for } 0<r<a,\ 0<z<a,$$

$$\frac{\partial}{\partial t}[T(\underline{\mathbf{x}},0)]\bigg|_{t=0}=0 \text{ for } 0<r<a,\ 0<z<a,$$

$$\underline{\mathbf{q}}(\underline{\mathbf{x}},0)=0 \text{ for } 0<r<a,\ 0<z<a,$$

and the boundary conditions

$$q(r,a,t)=0 \text{ for } 0<r<a,\ t>0,$$

$$q(a,z,t)=0 \text{ for } 0<z<a,\ t>0,$$

$$q(r,0,t)=0 \text{ for } r_c<r<a,\ t>0,$$

$$q(r,0,t)=-(H(t)-H(t-\tau_0))q_0 \text{ for } 0<r<r_c,\ t>0,$$

where q_0 is the magnitude of the specified heat flux, τ_0 is the duration of the heating on the surface $z = 0$ and H denotes the unit-step Heaviside function.

To solve this particular problem for the non-dimensionalized temperature $\kappa_0(T - T_0)/(aq_0)$, it is sufficient to input the five non-dimensionalized parameters which are listed below:

τ_T/τ_q(non-dimensionalized phase in temperature gradient)

τ_0/τ_q(non-dimensionalized duration of surface heating)

$a\sigma$(non-dimensionalized grading parameter of thermal properties)

r_c/a(non-dimensionalized radius of the region of heating)

$\kappa_0\tau_q/(a^2\rho_0 c_0)$(non-dimensionalized thermal diffusivity)

If the radius a of the solid cylinder is several centimeter long (for example, a = 0.05 m) and κ_0, ρ_0 and c_0 are respectively the values of the thermal conductivity, density and specific heat of a typical biological tissue with (for example) phase lag $\tau_q = 16s$ then $\kappa_0\tau_q/(a^2\rho_0 c_0)$ may have a magnitude of the order 10^{-3} (see Zhou, Zhang and Chen, 2009). Taking $\kappa_0\tau_q/(a^2\rho_0 c_0) = 10^{-3}$ and $r_c/a = 0.2$, we examine the effects of varying the non-dimensionalized parameters τ_T/τ_q and $a\sigma$ on the non-dimensionalized temperature $\kappa_0(T - T_0)/(aq_0)$for cases in which the material is subject to a short duration of surface heating (with $\tau_0/\tau_q = 0.1$)and continuous heating (with $\tau_0/\tau_q \to \infty$) respectively.

To carry out the numerical simulation with good accuracy, the boundary of the solution domain is discretized into 150 elements and 945 collocation points are placed in the interior of the solution domain. To model the rapid change in temperature distibution in the region near where the surface $z = 0$ is subject to heating, most of the interior collocation points are concentrated within a small region near $(r,z) = (0,0)$. More specifically, 729 collocation points are placed in the region $0 < r < 0.01a$, $0 < z < 0.01a$, and the other 216 points are distributed evenly in the remaining part of the solution domain. For the numerical inversion of the Laplace transform solution, $M = 8$ is used in the Stehfest's formula in (39).

For $a\sigma = 0$ (homogeneous solid), $\tau_0/\tau_q = 0.1$ (short duration heating on the surface $0 < r < r_c$, $z = 0$) and some selected values of τ_T/τ_q, the non-dimensionalized temperature $\kappa_0(T - T_0)/(aq_0)$ at $(r/a, z/a) = (0,0)$ is plotted against t/τ_q in Fig. 6. For each τ_T/τ_q, the non-dimensionalized temperature $\kappa_0(T(0,0,t) - T_0)/(aq_0)$ reaches its maximum value just before the end of the heating on the surface $0 < r < r_c$, $z = 0$ (that is, at around $t = 0.095\tau_q < \tau_0$). From Fig. 6, it is apparent that $\kappa_0(T(0,0,t) - T_0)/(aq_0)$has a higher maximum value, is more oscillatory in time and is slower in approaching the steady state $(T = T_0)$ for τ_T/τ_q with a smaller magnitude. Thus, it appears that a larger value of τ_T/τ_q has a greater damping effect on the thermal wave response in the solid, as may perhaps be expected.

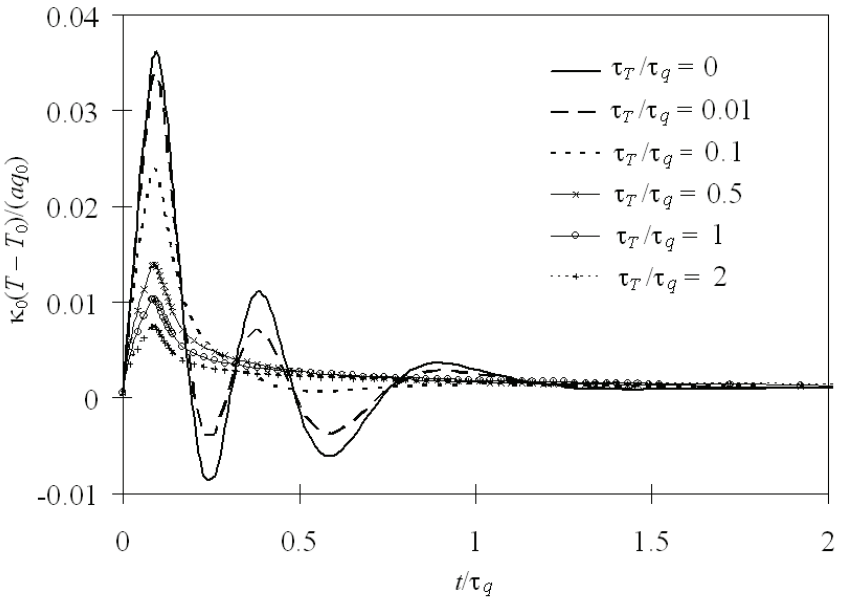

Figure 6: Plots of the non-dimensionalized temperature at the center of heating against t/τ_q for selected values of τ_T/τ_q (short duration heating).

To examine the effect of the non-dimensionalized parameter $a\sigma$ on the heating of the cylindrical solid, we now consider the case of continuous heating on the surface $0 < r < r_c$, $z = 0$ ($\tau_0/\tau_q \to \infty$) with $\tau_T/\tau_q = 0.01$. The non-dimensionalized temperature $\kappa_0(T-T_0)/(aq_0)$ at $(r/a, z/a) = (0,0)$ is plotted against t/τ_q in Fig. 7 for selected values of $a\sigma$. For time $t/\tau_q < 0.1$, the graphs of $\kappa_0(T(0,0,t)-T_0)/(aq_0)$ appear to be almost indistinguishable for $a\sigma = -3$, $a\sigma = 0$ and $a\sigma = 3$. The difference in the temperature $\kappa_0(T(0,0,t)-T_0)/(aq_0)$ for the three selected values of $a\sigma$ only becomes more obvious as time evolves. To show this for the temperature at other points inside the solid, the spatial variation of $\kappa_0(T-T_0)/(aq_0)$ on $r/a = 0$ with z/a (for $0 < z/a < 0.1$) is examined in Fig. 8 at time $t/\tau_q = 0.1$, $t/\tau_q = 0.5$, $t/\tau_q = 1$and $t/\tau_q = 2$. At small time $t/\tau_q = 0.5$, the difference in the non-dimensionalized temperature $\kappa_0(T(0,z,t)-T_0)/(aq_0)$ for each of the three cases $a\sigma = -3$, $a\sigma = 0$ and $a\sigma = 3$ is obvious only for a very small range z/a near the center of the surface heating. The difference becomes more pronounced over an increasing larger range of z/a as time increases. Fom Fig. 7 and 8, it is apparent that as time evolves the temperature for $a\sigma = 0$ (homogeneous solid) will become lower than that for $a\sigma = -3$ but higher than that for $a\sigma = 3$ over an

increasingly larger region of the solid.

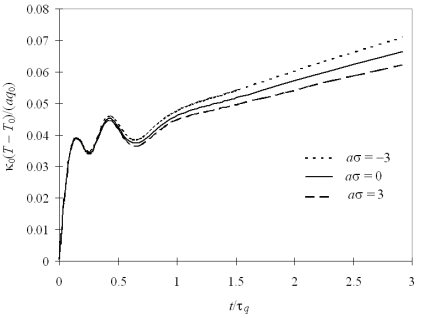

Figure 7: Plots of the non-dimensionalized temperature at the center of heating against t/τ_q for τ_T/τ_q= 0.01 and selected values of $a\sigma$ (continuous heating).

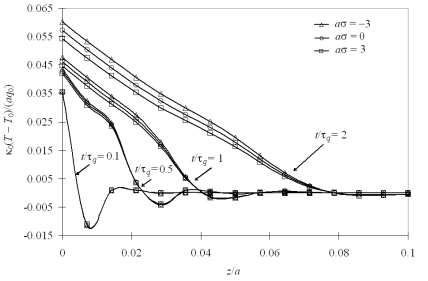

Figure 8: Plots of non-dimensionalized temperature against z/a at for τ_T/τ_q=0.01 and selected values of $a\sigma$ at various time instants (continuous heating).

7 Summary

The numerical simulation of axisymmetric dual-phase-lag heat conduction in non-homogeneous thermally isotropic solids is considered. The temperature field is obtained numerically by using a dual-reciprocity boundary element method to solve the governing partial differential equation in the Laplace transform domain. The task of determining the temperature field is eventually reduced to solving a system of linear algebraic equations. Once the linear algebraic equations are solved, the physical temperature can be recovered by using a numerical algorithm for inverting Laplace transform.

The numerical approach presented is applicable for nonhomogeneous solids with thermal conductivity, density and specific heat which are given by rather general functions of the axisymmetrical spatial coordinates. Through the use of appropriate interpolating functions, the domain integral which arises in the integral formulation of the problem is approximated in terms of integral over the boundary of the solution domain. Thus, in the numerical implementation, only the boundary of the solution domain has to be discretized into elements.

To assess the validity and accuracy of the proposed numerical procedure, some test problems which have known solutions are solved. The numerical solutions obtained indicates that the dual-reciprocity boundary element method presented can be used as a reliable and accurate computational tool for analyzing axisymmetric

dual-phase-lag heat conduction in nonhomogeneous solids. The method is also applied to simulate the heating of a particular exponentially graded cylindrical solid. The effects of the spatial variations of the thermal properties and the phase lags in the temperature gradient and flux fields on the thermal behaviors of the solid are examined. The numerical results obtained appear to be intuitively and qualitatively acceptable.

References

Abramowitz, M.; Stegun, I. (1970): *Handbook of Mathematical Functions*. Dover, New York.

Ang, W. T. (2002): A Laplace transformation dual-reciprocity boundary element method for a class of two-dimensional microscale thermal problems. *Engineering Computations*, vol. 19, pp. 467-478.

Antaki, P. J. (1998): Solution of non-Fourier dual phase lag heat conduction in a semi-infinite slab with surface heat flux. *International Journal of Heat and Mass Transfer*, vol. 41, pp. 2253-2258.

Azis, M. I.; Clements D. L.; Budhi, W. S. (2003): A boundary element method for the numerical solution of a class of elliptic boundary value problems for anisotropic inhomogeneous media. *ANZIAM Journal*, vol. 44, pp. C79-C95.

Brebbia, C. A.; Nardini, D. (1983): Dynamic analysis in solid mechanics by an alternative boundary element procedure. *International Journal of Soil Dynamics and Earthquake Engineering*, vol. 2, pp. 228-233.

Brebbia, C. A.; Telles, J. C. F.; Wrobel, L. C. (1984): *Boundary Element Techniques, Theory and Applications in Engineering*. Springer-Verlag, Berlin/Heidelberg.

Dai, W.; Nassar, R. (1999): A finite difference scheme for solving solving the heat transport equation at the microscale. *Numerical Methods for Partial Differential Equations*, vol. 15, pp. 697-708.

Davies, B.; Martin, B. (1979): Numerical inversion of the Laplace transform: a survey and comparison of methods. *Journal of Computational Physics*, vol. 33, pp. 1-32.

Ding, S. H.; Li, X.; Zhou, Y. T. (2010): Dynamic stress intensity factors of mode I crack problem for functionally graded layered structures. *CMES: Computer Modeling in Engineering & Sciences*, vol. 56, pp. 43-84.

Divo, E.; Kassab, A. J. (1998): A generalized BIE for transient heat conduction in heterogeneous media. *AIAA Journal of Thermophysics and Heat Transfer*, vol. 12, pp. 364-373.

Kaminski, K. (1990): Hyperbolic heat conduction for materials with a nonhomo-

geneous inner structure. *ASME Journal of Heat Transfer*, vol. 112, pp. 555-560.

Manzari, M. T.; Manzari, M. T. (1998): A mixed approach to finite-element analysis of hyperbolic heat conduction problems. *International Journal for Numerical Methods in Heat and Fluid Flow*, vol. 8, 83-97.

Nerantzaki, M. S.; Kandilas, C. B. (2008): A boundary element method solution for anisotropic nonhomogeneous elasticity. *Acta Mechanica*, vol. 200, pp. 199-211.

Ochiai, Y.; Sladek, V.; Sladek, J. (2009): Axial symmetric elasticity analysis in nonhomogeneous bodies under gravitational load by triple-reciprocity boundary element method. *International Journal for Numerical Methods in Engineering*, vol. 78, pp. 779-799.

Pan, H.; Tang, D.; Zhou, L. (2006): Numerical analysis of two-dimensional lagging thermal behavior under short-pulse-laser heating on surface. *International Journal of Engineering Science*, vol. 44, pp. 1510-1519.

Paris, F.; Canas, J. (1997): *Boundary Element Method: Fundamentals and Applications*. Oxford University Press, Oxford.

Park, Y. S.; Ang, W. T. (2000): A complex variable boundary element method for an elliptic partial differential equation with variable coefficients. *Communications in Numerical Methods in Engineering*, vol. 16, pp. 697-703.

Partridge, P. W.; Brebbia, C. A.; Wrobel. L. C. (1992): *The Dual Reciprocity Boundary Element Method*. Computational Mechanics Publications, London.

Sladek, J.; Sladek, V.; Solek, P. (2009): Elastic analysis in 3D anisotropic functionally graded solids by MLPG. *CMES: Computer Modeling in Engineering & Sciences*, vol. 43, pp. 223-252.

Stehfest, H. (1970): Numerical inversion of the Laplace transform. *Communications of ACM*, vol. 13, pp. 47-49 (see also p624).

Tang, D. W.; Araki, N. (1991): Wavy, wavelike, diffusive thermal responses of finite rigid slabs to high-speed heating of laser-pulses. *International Journal of Heat and Mass Transfer*, vol. 42, pp. 855-860.

Tzou, D. Y. (1995): A unified field approach for heat conduction from micro- to macro-scales. *ASME Journal of Heat Transfer*, vol. 117, pp. 8-16.

Tzou, D. Y. (1997): *Macro- to Microscale Heat Transfer: The Lagging Behavior*. Taylor and Francis, Bristol.

Tzou, D. Y.; Chiu, K. S. (2001): Temperature-dependent thermal lagging in ultrafast laser heating. *International Journal of Heat and Mass Transfer*, vol. 44, pp. 1725-1734.

Wang, K.; Mattheij, R. M. M.; ter Morsche, H. G. (2003): Alternative DRM formulations. *Engineering Analysis with Boundary Elements*, vol. 27, pp. 175-181.

Yuen W. W.; Lee, S. C. (1989): Non-Fourier heat conduction in a semi-infinite solid subjected to oscillatory surface thermal disturbances. *ASME Journal of Heat Transfer*, vol. 11, pp. 178-181.

Yun, B. I.; Ang, W. T. (2010): A dual-reciprocity boundary element approach for axisymmetric nonlinear time-dependent heat conduction in a nonhomogeneous solid. *Engineering Analysis with Boundary Elements*, vol. 34, 697-706.

Zhang, J.; Zhao, J. J. (2001): Unconditionally stable finite difference scheme and iterative solution of two-dimensional microscale heat transport equation. *Journal of Computational Physics*, vol. 170, 261-275.

Zhang, Z. M. (2007): *Nano/Microscale Heat Transfer*. McGraw-Hill, New York.

Zhou, J.; Chen, J. K.; Zhang, Y. (2009): Dual-phase-lag effects on thermal damage to biological tissues caused by laser irradiation. *Computers in Biology and Medicine*, vol. 39, pp. 286-293.

Zhou, J.; Zhang, J.Y.; Chen, J. K. (2009): An axisymmetric dual-phase-lag bioheat model for laser heating of living tissues. *International Journal of Thermal Science,* vol. 48, pp. 1477-1485.